Journal of Nano- and Electronic Physics
Vol. **18** No 3, 03003(7pp) (2026)

Журнал нано- та електронної фізики
Том **18** № 3, 03003(7cc) (2026)

OPEN ACCESS

REGULAR ARTICLE

The Effect of the Interaction of Intense UV Radiation with Thin NZO Films

I.S. Virt[1,*], N.V. Barchuk[1,†], P. Potera[2,‡], M.V. Chekailo[3,§]

[1] *Drohobych Ivan Franko State Pedagogical University, 82100 Drohobych, Ukraine*
[2] *University of Rzeszow, 35-310 Rzeszow, Poland*
[3] *Lviv Polytechnic National University, 79000 Lviv, Ukraine*

(Received 13 April 2026; revised manuscript received 19 June 2026; published online 26 June 2026)

This study investigates the physical properties of nickel-doped zinc oxide (NZO) thin films fabricated via pulsed laser deposition (PLD) on both rigid and flexible substrates. Post-growth modification was performed using ultraviolet (UV) photonic annealing, and the impact of processing conditions on the microstructural, electrical, and optical properties of the resulting NZO nanostructures was systematically evaluated. Our findings demonstrate that photonic annealing induces significant crystalline transformations throughout the bulk and surface of the films. Optimal irradiance levels were identified at 20 kJ/cm² for rigid substrates and 36 kJ/cm² for flexible ones, enabling the fabrication of nanostructured surfaces with tailored characteristics. The ability to modulate these properties by adjusting photon flux and exposure time highlights UV annealing as a viable low-temperature technique for flexible electronics. Furthermore, the observed reduction in oxygen-related defects correlates with the measured optoelectronic behavior, validating established models for ZnO defect chemistry. These results provide a robust foundation for the development of high-performance flexible photosensors and compatible bioelectronic devices.

Keywords: Zinc oxide, Thin films, Photonic annealing, Surface morphology, Electrophysical properties, Photovoltaic, Optical characteristics.

DOI: 10.21272/jnep.18(3).03003 PACS numbers: 61.80.Ba, 61.82.Fk, 71.55.Gs

1. INTRODUCTION

Zinc oxide (ZnO) has emerged as a key material for transparent conductive coatings, which are essential for applications such as photovoltaic cells, solid-state lighting, and transparent transistors [1]. Its prominence in the field is attributed to a unique combination of high optical transparency, piezoelectricity, and cost-effectiveness. Characterized by a wide direct band gap of 3.27 eV and a high room-temperature exciton binding energy (60 meV), ZnO is particularly well-suited for electronics and optoelectronics [2]. Furthermore, its capacity for self-organized growth facilitates the fabrication of various nanostructures using techniques like thermal or chemical deposition, sol-gel methods, and laser sputtering, making it indispensable for sensors and display technologies [3, 4].

Optimizing the structural characteristics of ZnO is crucial for achieving high performance in optoelectronic devices. Current strategies for structural modification include plasma irradiation, chemical reactions, and thermal treatments. However, a significant challenge remains: achieving superior crystallinity with minimal defect density typically necessitates high-temperature growth or post-annealing (> 400 °C) [5, 6]. Such conventional furnace treatments are incompatible with heat-sensitive plastic substrates, leading to increased production costs and technical complexity. Consequently, the integration of ZnO nanostructures into flexible electronics, wearable biosensors, and foldable medical displays remains restricted [7, 8]. While Pulsed Laser Deposition (PLD) allows for the fine-tuning of properties via dopant concentration, substrate temperature, and gas composition [9], there is a growing need for alternative post-deposition techniques to induce oxygen deficiency without compromising substrate integrity.

In contrast, photonic annealing offers a highly efficient alternative by facilitating rapid, localized thermal processing with negligible energy loss. This technique enables selective treatment of specific areas while preserving the integrity of the underlying substrate and adjacent structures. The efficacy of photonic annealing is primarily governed by parameters such as radiation flux density, photon energy, and exposure duration. Notably, excimer laser annealing has been successfully employed to enhance the crystalline and electrical characteristics of ZnO films, leveraging strong ultraviolet absorption even at low ambient temperatures [10]. While several studies have elucidated the mechanisms of laser-induced modification in ZnO thin films [11, 12], it is established that the irradiated energy density directly influences recrystallization and nanostructural evolution. However, caution is required, as excessive

* Correspondence e-mail: isvirt@dspu.edu.ua
† nazar.barchuk@gmail.com
‡ ppotera@ur.edu.pl
§ mykola.v.chekailo@lpnu.ua

Cite this article as: I.S. Virt, et al., *J. Nano- Electron. Phys.* 18 No 3, 03003 (2026) https://doi.org/10.21272/jnep.18(3).03003

irradiation of metal oxide films can lead to irreversible structural damage and subsequent optical degradation [13]. Furthermore, long-wavelength continuous high-power irradiation has proven effective for local surface smoothing of optical materials.

The methodology presented in this study utilizes photon irradiation on deposited films with low conductivity, employing energy levels that surpass the band gap. At these energies, metal-oxygen bonds become susceptible to dissociation. This approach is based on a significant body of published work on the interaction of high-energy light pulses with optical thin films [14]. High-energy irradiation of thin optical films frequently results in catastrophic failure, primarily driven by linear and nonlinear absorption at structural defect sites. Conversely, exposure below the critical damage threshold often induces material densification and subtle shifts in optical characteristics. This phenomenon is particularly significant in amorphous films, where radiation-induced crystallization can be leveraged to fabricate specialized structures or to substantially modify material properties for microsensor applications [15].

2. EXPERIMENTAL DETAILS

2.1 Thin Film Synthesis

The aim of the work described in this paper is to investigate the induced changes in nickel-doped zinc oxide films exposed to UV radiation in air. To achieve these changes, this work uses irradiation of doped zinc oxide films at energies exceeding the band gap. Under these conditions, almost all of the beam energy is absorbed by the film and is only weakly transmitted to the film–substrate interface. Short-wave irradiation of metal oxide films exceeding the band gap also stimulates photoconductivity by promoting electrons from trap states into the conduction band. The decay of induced photoconductivity can occur over long time scales.

2.2 Photonic Processing of Thin Films

The growth of doped ZnO thin films was carried out using pulsed laser deposition (PLD) technology. PLD technology has already been demonstrated for the growth of one-dimensional ZnO nanostructures [16] and for deposition at relatively low temperatures (< 100 °C) on flexible plastic substrates [17]. The PLD method involves the use of laser radiation to eject materials from the surface of a target, which are then deposited onto the substrate. This results in stoichiometric coatings, both single-layer and multilayer, with specified properties. Experimental PLD system developed and used for material deposition. A $KGd(WO_4)_2$ laser was used. Radiation characteristics: $\lambda = 1067$ nm, pulse duration $t = 20$ ns, beam energy density $6 \div 8$ J/cm^2, repetition rate $1.0 \div 0.3$ Hz. The technological module uses a Q–switch for irradiation in the Q–modulation mode. Ablation of pressed polycrystalline targets was carried out in a quartz chamber. The final pressure in the deposition chamber was 10^{-6} Pa. Silicon (111) Si and polymer were used as substrates. The deposition temperature (substrate temperature) was about 200 °C. Thin films were obtained with an area of 1×1 cm^2. Successive layers were deposited under the same conditions. The average film thickness was ~ 300 nm for NZO (nickel-doped zinc oxide). The sputtered films were dielectric. To overcome this problem, we applied ultraviolet annealing to improve the structural quality of NZO without affecting the underlying polymer substrate. Annealing is a well-known technique used in semiconductor thin film processing to locally recrystallize materials without melting the substrate (e.g., polysilicon) [18]. Rapid irradiation in the range of a few tens of minutes allows for recrystallization and removal of defects, thus enhancing the optical and electronic characteristics of the material without affecting its quality.

In this work, we propose to combine PLD deposition with photonic annealing to obtain high-quality NZO nanostructures. By combining PLD with photonic annealing, we propose a new technique fully compatible with flexible substrates that exploit the advantages of low temperatures. We demonstrate that photonic annealing of NZO creates a unique topography of nanostructured films with high surface area that can be functionalized and used for biosensors in particular.

There are two steps for the deposition of NZO thin films: thin film coating and photonic processing. A 365 nm LED with a maximum energy density of approximately 10 W/cm^2 was used. NZO samples were irradiated with different energy densities from 1 kJ/cm^2 to 36 kJ/cm^2 in air, without additional heating of the substrate. The effect of irradiation on the structural properties of NZO was evaluated by scanning electron microscopy using an Apreo 2C LoVac scanning electron microscope (Thermo Fisher Scientific) at room temperature.

3. RESULTS

3.1 Analysis of Surface Morphology of NZO Films

Scanning Electron Microscopy (SEM) was employed to evaluate morphological transitions, focusing on surface roughness and uniformity. Measurements were conducted across various sample regions, specifically comparing nanostructured NZO grown on Si substrates in their as-grown state versus those irradiated at 36 kJ/cm^2. Despite all samples maintaining the characteristic ZnO wurtzite crystal structure [19], distinct morphological variations were observed between the analyzed areas. Similar experiments performed on flexible polyimide substrates revealed significant structural modifications correlating with increased irradiation energy density (Fig. 1 a-d). Notably, photon annealing resulted in a more homogeneous and planar surface morphology compared to the pristine films. This transformation is attributed to the partial degradation of grain boundaries during annealing, followed by propagation into the grains, which facilitates the formation of a fine crystalline structure. While low radiation doses had negligible effects on NZO nanorods on Si substrates, a critical process window was identified between 15 and 36 kJ/cm^2, within which dramatic morphological shifts occur.

The SEM analysis of the as-deposited thin films revealed a dense surface characterized by irregularly shaped grains with an average size of 62.4 nm. Following irradiation, these grains transitioned to a more rounded morphology. Notably, the grain size in sample 1c was

substantially reduced to 16.1 nm, accompanied by a significant decrease in surface roughness and the attainment of exceptional flatness and density. Grain size distribution histograms confirm a strong dependence on photon flux: as the flux increases, the distribution peak shifts toward smaller dimensions and the distribution range narrows. These modifications on rigid substrates are attributed to the targeted impact on intraband defects, as corroborated by [20].

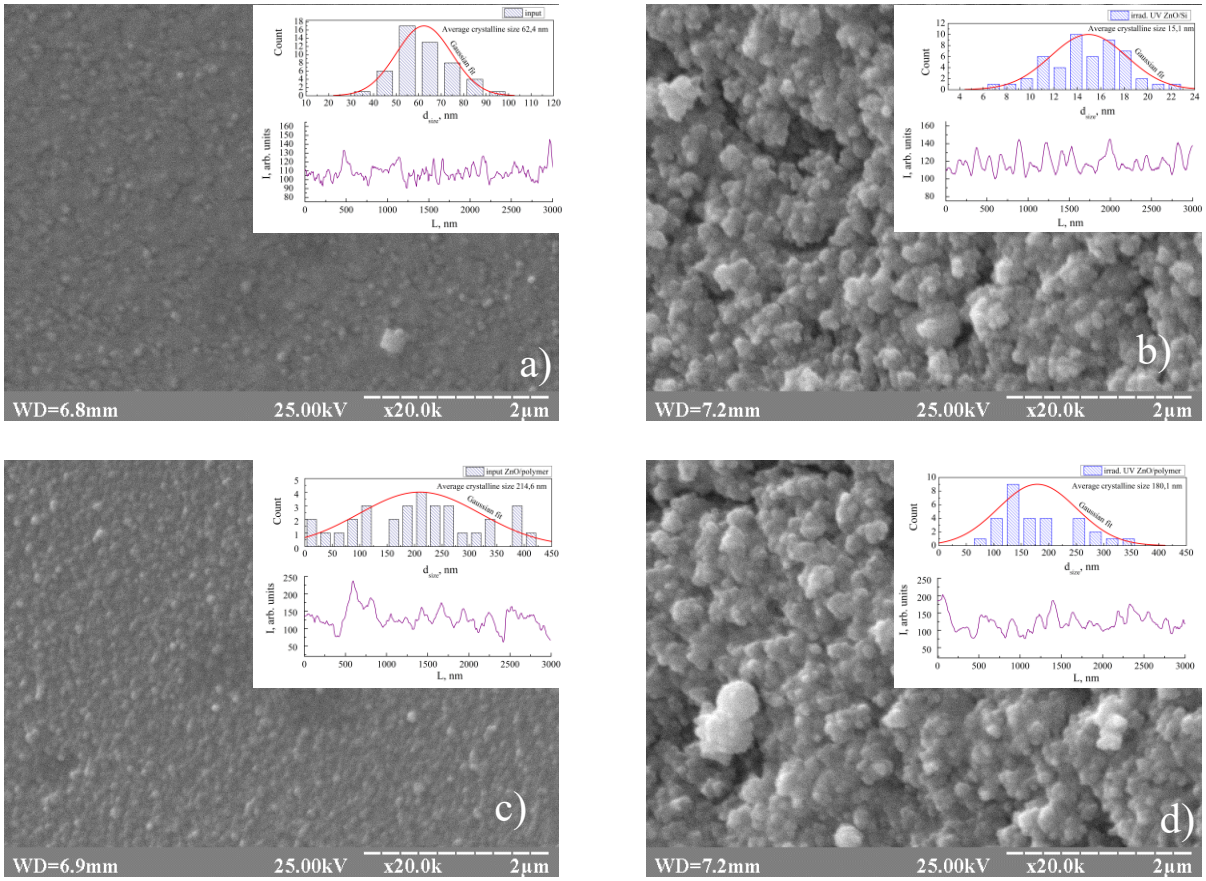

Fig. 1 – SEM images of the surface of a nanostructured NZO film grown on top of Si – a) and polymer – b), irradiated at 36 kJ/cm² – c), d). Insets: corresponding histograms of average grain sizes and surface morphology profile of films

In contrast to NZO nanorods on silicon, the 'healing' of surface defects on polymer substrates becomes prominent only at a power density of 20 kJ/cm². The initial grain size of 214.6 nm (Fig. 1b) was reduced to 180.1 nm (Fig. 1d) post-irradiation, signifying the elimination of internal defects such as oxygen vacancies (V_O) and zinc interstitials (Zn_i) [21, 22]. Furthermore, the reduction in grain size increases the volume fraction of grain boundaries [23]. Ultimately, photon irradiation serves as a critical tool for modulating grain size, density, and crystallinity – parameters that fundamentally determine the film's conductivity and grain boundary behavior.

3.2 Effect of Irradiation on the Electrical Properties of Thin Films

Fig. 2 shows the variation of electrical conductivity σ with the reciprocal of temperature $1/T$ ($\sigma(T)$). The observed decrease in film resistance with rising temperature confirms the semiconducting behavior of all prepared samples. Notably, the electrical conductivity of the irradiated NZO thin films was superior to that of the as-deposited layers. Photon irradiation significantly modulated the electrical properties, with sample – 2 exhibiting a slight increase in conductivity compared to sample – 1 (Fig. 2). Activation energies (E_D) were derived from the slope of the Arrhenius plots in their linear regimes. As illustrated in Fig. 2, the activation energy for the irradiated NZO films is substantially lower than that of the unirradiated control, aligning with previously reported ΔE values for NZO. In these n-type semiconductors, conductivity is governed by the excitation of free carriers from defect levels situated near the conduction band [24].

The resulting conductivity is a function of both carrier concentration and mobility, which typically exhibit an inverse relationship [25]. It has been documented that films with high crystallinity tend to possess a lower density of charge carriers, such as electrons, whereas films with reduced crystallinity often exhibit a higher carrier concentration [26].

Increasing the cation concentration leads to an increase in the degree of electron localization, so the activation energy will decrease with an increase in the number of donor sites [27]. The resistivity R decreased with increasing photon flux density, which was explained by the improvement due to the decrease in the number of O vacancies (V_O). The conductivity of the film increased from 0.014 to 0.032 (1/(Ohm·cm) at room temperature.

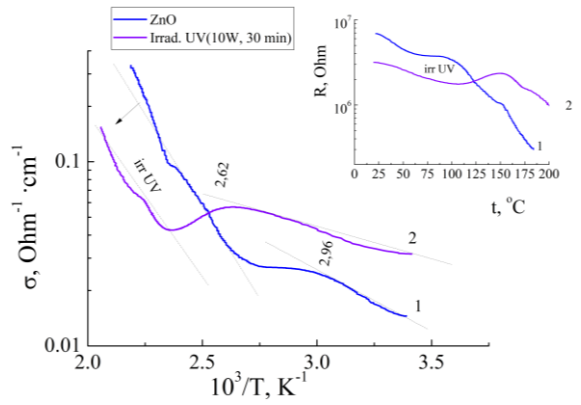

Fig. 2 – Temperature dependence of the electrical conductivity of a nanostructured NZO film grown on top of a polymer: unirradiated – (1) and irradiated at 36 kJ/cm² – (2). Inset: corresponding temperature dependences of electrical resistance

The temperature dependence of the conductivity can be described by the Arrhenius equation, which is defined as:

$$\sigma(T) = \sigma_0 \cdot \exp\left(\frac{E_D}{kT}\right) \quad (1)$$

where σ, T, σ_0 and k – are the conductivity, temperature, the dimensional constant of the conductivity and the Boltzmann constant, respectively. The observed reduction in activation energy (E_D) may be attributed to an increased density of vacancies or structural defects. Specifically, high photon flux levels likely facilitate the generation of donor-type defects, thereby enhancing electrical conductivity. Simultaneously, irradiation-induced modifications in grain size significantly alter the volume fraction of grain boundaries. As grain size diminishes, the boundary volume fraction increases accordingly. Consequently, irradiation serves as a critical factor in modulating key film parameters – such as grain size, density, and crystallinity – which fundamentally dictate conductivity and grain boundary behavior [28, 29]. Furthermore, the decrease in effective roughness, as determined by the effective medium approximation (EMA), suggests a correlation with these distinctive morphological transitions.

To evaluate the optical band gap (E_g) and the overall optical quality of the NZO thin films, transmittance spectra were recorded at room temperature across a wavelength range of 180 to 3300 nm (Fig. 3). The films deposited on polymer substrates exhibited high transparency in the near-infrared (NIR) region, with average transmission values ranging from 75 % to 83 %. The presence of distinct, well-defined interference fringes in the spectra confirms the high degree of thickness uniformity across the deposited layers. These patterns result from the constructive and destructive interference of multiple light reflections, driven by the refractive index contrast between the film and the substrate. Since the efficiency of photovoltaic devices is fundamentally linked to the material's photon absorption capacity – determined by the relationship between incident photon energy and the optical band gap – accurate determination of E_g is essential. The absorption coefficient (α), which characterizes electron transitions from the valence band to the conduction band, is calculated using the following relation:

$$\alpha = \frac{1}{d} \cdot \ln\left(\frac{1}{T}\right) \quad (2)$$

where d is the thickness in [cm], T% is the transmittance of the sample.

We determined the E_g of NZO thin films using the Tauc relation [30]:

$$\alpha \cdot h\nu = B \cdot (h\nu - E_g)^m \quad (3)$$

where B is a constant, h is Planck's constant, ν is the photon frequency, and m is an index that can take the value 0.5 for direct allowed transitions observed for ZnO [30].

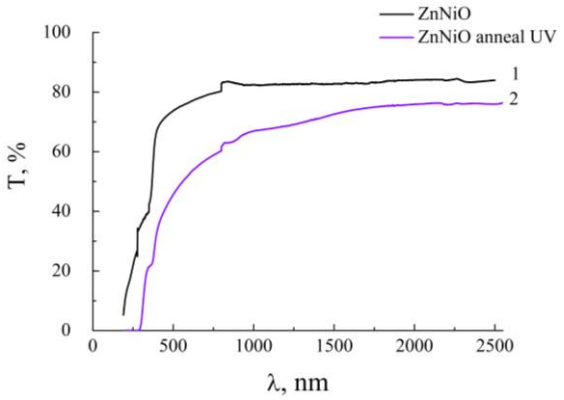

Fig. 3 – Spectral dependence of the transmittance of the NZO film grown on top of the polymer: unirradiated – (1) and irradiated at 36 kJ/cm² – (2)

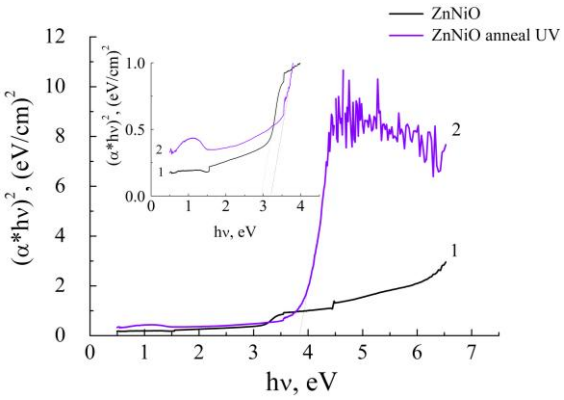

Fig. 4 – Spectral dependence of the absorption coefficient of the NZO film grown on top of the polymer: unirradiated – (1) and irradiated at 36 kJ/cm² – (2)

The optical band gap E_g of the films can be determined using the graph $(\alpha h\nu)^2 = f(h\nu)$, based on the intersection of the continuation of the straight part of the curves with the $h\nu$ axis (Fig. 4). Although the increase in the UV range can be explained by the migration of Zn_i to the surface, the source of the decrease in the visible range should be sought in the deeper region. In particular, since the intensity of the visible range is dominated by surface defects, this is consistent with the removal of oxygen defects, which occurs with the reduction of some ZnO on the surface itself.

The fundamental characteristics of the photoconductivity process in the synthesized films are illustrated in Figs. 5, 6. Specifically, Fig. 5 presents the time-resolved decay curves of the NZO layers under photoexcitation at λ = 365 nm. When excitation occurs within

the fundamental absorption region, light quanta penetrate only to a shallow depth; consequently, the transport dynamics of non-equilibrium charge carriers are primarily governed by their interaction with major scattering centers and lattice defects. The temporal evolution of the carrier lifetime can be accurately modeled using multi-exponential approximations."

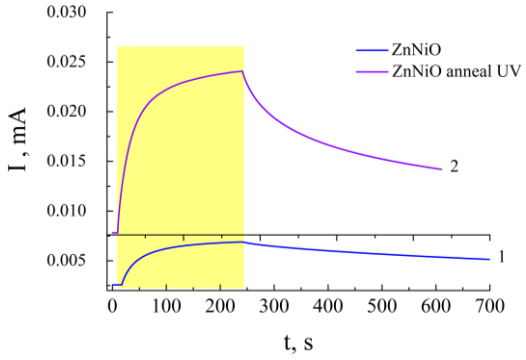

Fig. 5 – Time dependence of the photocurrent (under the action of LED illumination $\lambda = 365$ nm) of a thin NZO film – (1) and a UV-irradiated film – (2)

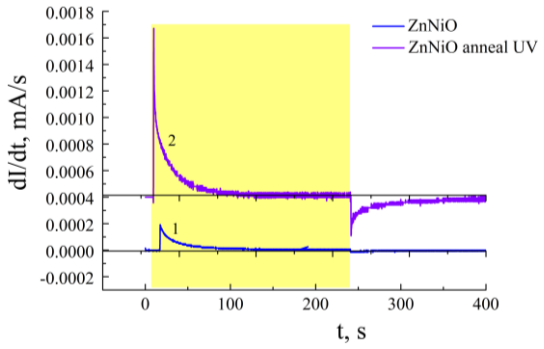

Fig. 6 – Kinetics of the value of the derivative of the photocurrent in the coordinates $dI_{ph}/dt \div t$ of a thin NZO film – (1) and a UV– irradiated film – (2)

In our case, we have plotted the derivative of the photocurrent with respect to the logarithm of time: $dI(t)/dt$. Differentiation with respect to the time parameter gives peaks at $t = \tau$ (Fig. 6), and these peaks demonstrate asymmetry and some broadening. In particular, the relaxation time parameter reflects the broadening of the curve (Fig. 6), and its value is determined by the magnitude of the potential barrier fluctuations involved in the capture of charge carriers [31]. This is different from the case of a perfect exponential decay [32, 33].

Under illumination, the photocurrent evolution is characterized by three distinct stages: an initial rapid rise with a relaxation time of 0.41 s, followed by a slower growth phase with a characteristic time of 55 s, and a subsequent decay period (relaxation time: 0.35 s). The observed peaks are notably broad, exceeding the expectations for standard exponential growth [34, 35]. Following the initial fast decay, the photocurrent exhibits a persistent tail with a time constant of approximately 120 s, which is accurately modeled by a stretched exponential function. The prevalence of stretched exponents over simple ones suggests a transport mechanism governed by capture centers with potential barriers or significant potential fluctuations. Developing a comprehensive recombination model for these semi-insulating photoconductive detectors necessitates further investigation.

4. DISCUSSION

Although a clear understanding of the interaction of high-energy radiation with solid surfaces has not yet been achieved, significant progress in improving the mechanisms that explain the damage phenomenon is evident. Central to this argument is the requirement for the presence of free electrons in the conduction band of the material. It has been shown in [36] that pulsed ultraviolet irradiation of silicon dioxide above a critical threshold leads to the emission of negative ions, such as O-, positive ions, and neutrals from the material. The resulting defect states created in the oxide will modify the permanent electrical and optical properties [37, 38]. The results presented in our paper are consistent with this work and suggest that irradiation of oxide films at energies exceeding the band gap can break the chemical bond in such a way that free electrons from defect states can be introduced into the conduction band. The significant increase in the film conductivity upon photon irradiation was also accompanied by perturbations in the measured transmission, which support the claim that the release of oxygen from the lattice introduces free electron carriers into the conduction band. Similar effects were observed in zinc oxide films that were electrochemically reduced and then reoxidized, or in films that were reduced with hydrogen at elevated temperatures and then reoxidized by heating in air [39]. It was observed that the photon–induced generation of oxygen vacancies reduces the resistivity of the films and changes the band gap energies. As can be seen from our results, upon irradiation of the films, their effective conductivity increases by a factor of two. The increase in σ can be explained by the photon–induced migration of Zn_i to the surface region and the reduction of surface defects with a subsequent increase in the mobility of free electrons. These shallow donors can compensate for the electron accumulation layer on the surface, which is known to strongly affect the electrical properties of ZnO [40]. These transport mechanisms involve the interaction of charge carriers with barriers to electron capture and/or a significant potential for their fluctuations.

5. CONCLUSIONS

In summary, we have demonstrated a novel approach for the synthesis and structural modification of ZnO (NZO) nanostructures on both rigid and flexible substrates. Our investigation into photonic annealing revealed a specific process window that yields uniformly distributed nanostructures with minimal macrodefects. The results indicate that photonic treatment significantly reconfigures the crystal structure both in the bulk and at the surface, which in turn dictates the film's electrical and optical performance. We identified optimal irradiance levels of 20 kJ/cm^2 for rigid substrates and 36 kJ/cm^2 for flexible substrates to fabricate nanostructured surfaces with tailored properties. Crucially, ultraviolet annealing emerges as a viable low-temperature processing technique for flexible electron-

ics. By controlling the parameter space of photon flux and exposure time, we successfully reduced oxygen-related defects, consistent with established theoretical models for ZnO. These findings provide a robust foundation for the advancement of next-generation flexible sensors and wearable bioelectronics.

REFERENCES

1. L. Liu, K. Cao, S. Chen, W. Huang, *Adv. Opt. Mater.* **8**, 2001122 (2020) https://doi.org/10.1002/adom.202001122.
2. D.K. Sharma, S. Shukla, K.K. Sharma, V. Kumar, *Mater. Today* **49** No 8, 3028 (2022) https://doi.org/10.1016/j.matpr.2020.10.238.
3. S. Vyas, *Johnson Matthey Technol. Rev.* **64** No 2, 202 (2020) https://doi.org/10.1595/205651320X15694993568524.
4. B.S.-H.K. Park, C.-S. Hwang, M. Ryu, S. Yang, C. Byun, J. Shin, J.-I. Lee, K. Lee, M.S. Oh, S. Im, *Adv. Mater.* **21**, 678 (2009) https://doi.org/10.1002/adma.200801470.
5. N.-ur-Rehman, M. Mehmood, S.M. Ali, S.M. Ramay, M.A. Shar, M.S. AlGarawi, *Appl. Phys. A* **125**, 528 (2019) https://doi.org/10.1007/s00339-019-2802-7.
6. P. Kumar, Nisha, P. Sarkar, S. Singh, B.C.K. Mishra, R.S. Katiyar, *Appl. Phys. A* **128**, 372 (2022) https://doi.org/10.1007/s00339-022-05511-2.
7. Y. Liu, K. Liu, J. Yang, Z. Cheng, X. Chen, Y. Zhu, B. Li, L. Liu, D. Shen, *J. Mater. Chem. C* **12**, 9623 (2024) https://doi.org/10.1039/D4TC01327A.
8. J. Theerthagiri, S. Salla, R.A. Senthil, P. Nithyadharseni, A. Madankumar, P. Arunachalam, T. Maiyalagan, H.-S. Kim, *Nanotechnology* **30** No 39, 392001 (2019) https://doi.org/10.1088/1361-6528/ab268a.
9. A.M. Mostafa, *Plasmonics* **20**, 5627 (2025) https://doi.org/10.1007/s11468-024-02706-6.
10. C.-Y. Tsay, M.-C. Wang, *Ceram. Int.* **39**, No 1, 469 (2013) https://doi.org/10.1016/j.ceramint.2012.06.050.
11. H. Palneedi, J.H. Park, D. Maurya, M. Peddigari, G.T. Hwang, V. Annapureddy, J.W. Kim, J.J. Choi, B.D. Hahn, S. Priya, K.J. Lee, J. Ryu, *Adv. Mater.* **30** No 14, 1870094 (2018) https://doi.org/10.1002/adma.201870094.
12. L.J. Wang, G.J. Exarhos, *Thin Solid Films* **519**, 1495 (2010) https://doi.org/10.1016/j.tsf.2010.04.118.
13. N. Nedyalkov, M. Koleva, R. Nikov, P. Atanasov, Y. Nakajima, A. Takami, A. Shibata, M. Terakawa, *Appl. Surf. Sci.* **374**, 172 (2016) https://doi.org/10.1016/j.apsusc.2015.10.216.
14. R.K. Singh, J. Narayan, *Phys. Rev. B* **41**, 8843 (1990) https://doi.org/10.1103/PhysRevB.41.8843.
15. H. Palneedi, J. Hwan Park, D. Maurya, M. Peddigari, G.-T. Hwang, V. Annapureddy, J.-W. Kim, J.-J. Choi, B.-D. Hahn, *Adv. Mater.* **30** No 14, 1705148 (2018) https://doi.org/10.1002/adma.201705148.
16. A. Ganguly, S. Chattopadhyay, K.-H. C. L.-C. Chen, *Nanostructures* **39** No 2 (2014).
17. S. Pal, S. Ghosh, D. Basak, *J. Mater. Sci.: Mater. Electron.* **32**, 16682 (2021) https://doi.org/10.1007/s10854-021-06224-7.
18. L. Rebohle, S. Prucnal, W. Skorupa, *Semicond. Sci. Technol.* **31** No 10, 103001 (2016) https://doi.org/10.1088/0268-1242/31/10/103001.
19. A.M. Mohammad, H.S. Ahmed Al-Jaf, H.Sh. Ahmed, M.M. Mohammed, Z.T. Khodair, *J. Ovonic Res.* **8** No 3, (2022) https://doi.org/10.15251/JOR.2022.183.443.
20. B. Clarke, K. Ghandi *Small* **19**, 2302864 (2023) https://doi.org/10.1002/smll.202302864.
21. G. Fiaschi, S. Mirabella, G. Franzò, L. Maiolo, A. Chitu, Y. Komemd, Y. Shacham, *Appl. Surface Sci.* **458**, 800 (2018) https://doi.org/10.1016/j.apsusc.2018.07.092.
22. K. Kim, S. Kim, S.Y. Lee, *Curr. Appl. Phys.* **12**, 1088 (2012) https://doi.org/10.1016/j.cap.2012.01.013.
23. Y. Hou, A.H. Jayatissa, *Thin Solid Films*, **562**, 585 (2014) https://doi.org/10.1016/j.tsf.2014.03.089.
24. S.J. Pearton, D.P. Norton, K. Ip, Y.W. Heo, T. Steiner, *J. Vac. Sci. Technol. B* **22**, 932 (2004) https://doi.org/10.1116/1.1714985.
25. T. Makino, Y. Segawa, A. Tsukazaki, A. Ohtomo, M. Kawasaki, *Appl. Phys. Lett.* **87**, 022101 (2005) https://doi.org/10.1063/1.1991994.
26. Y. Liu, Y. Li, H. Zeng, *J. Nanomater.* **2013** No 1, 196521 (2013) https://doi.org/10.1155/2013/196521.
27. Janotti, C.G. Van de Walle, *Phys. Rev. B* **76**, 165202 (2007) https://doi.org/10.1103/PhysRevB.76.165202.
28. Frechilla, J. Frechilla, L.A. Angurel, F. Toldrá-Reig, F. Balas, E. Martínez, G.F. de La Fuente, D. Muñoz-Rojas, *RSC Appl. Interfaces* **2** No 6, 1607 (2025) https://doi.org/10.1039/D5LF00076A.
29. S. Havlova, M. Novotny, P. Fitl, J. More-Chevalier, J. Remsa, V. Kiisk, M. Kodu, R. Jaaniso, P. Hruska, F. Lukac, J. Bulır, L. Fekete, L. Volfova, M. Vondracek, M. Vrnata, J. Lancok, *J. Mater. Sci.* **56**, 11414 (2021) https://doi.org/10.1007/s10853-021-06030-w.
30. I. Virt, P. Potera, R. Gamernyk, B. Cieniek, *Opt. Mater.* **154**, 115643 (2024) https://doi.org/10.1016/j.optmat.2024.115643.
31. L. Chen, S. Mao, P. Wang, Z. Yao, Z. Du, Z. Zhu, L.A. Belfiore, J. Tang, *Adv. Opt. Mater.* **9**, 2001505 (2021) https://doi.org/10.1002/adom.202001505.
32. Virt, R. Gamernyk, P. Potera, B. Cieniek, A. Lozynsky, *ECS J. Solid State Sci. Technol.* **11** No 6, 063013 (2022) https://doi.org/10.1149/2162-8777/ac765f.
33. G.H. Yu, X.W. Fan, Z.P. Guan, J.Y. Zhang, X.W. Zhao, D.Z. Shen, Z.H. Zheng, B.J. Yang, D.S. Jiang, Y.B. Chen, et al., *J. Electron. Mater.* **28** (1999).
34. V. Pecunia, J. Zhao, C. Kim, B.R. Tuttle, J. Mei, F. Li, Y. Peng, T.N. Huq, R.L.Z. Hoye, N.D. Kelly, et al., *Adv. Energy Mater.* **11**, 2003968 (2021) https://doi.org/10.1002/aenm.202003968.
35. N. Bouazizi, A. Abed, S. Girauda, A.E. Achari, C. Campagne, M.N. Morshed, O. Thoumire, R.E. Moznine, O. Cherkaoui, J. Vieillard, F.L. Derf, *Physica E: Low-Dimens. Syst. Nanostruct.* **118** No 113905 (2020) https://doi.org/10.1016/j.physe.2019.113905.
36. S. Zheng, Z. Chen, W.W. Duley, Y.A. Wu, P. Peng, Y.N. Zhou, *Nanotechnology* **34**, 495703 (2023) https://doi.org/10.1088/1361-6528/acf4a3.
37. Q. Xu, R.D. Hong, H.L. Huang, Z.F. Zhang, M.K. Zhang, X.P. Chen, Zh.Y. Wu, *Opt. Laser Technol.* **45**, 513 (2013) https://doi.org/10.1016/j.optlastec.2012.06.001.
38. L.J. Wang, G.J. Exarhos, *Thin Solid Films*, **519** No 5, 1495 (2010) https://doi.org/10.1016/j.tsf.2010.04.118.
39. H.J. Al-Asedy, S.A. Al-khafaji, S.K. Ghoshal, *Opt. Mater.* **115**, 111028 (2021) https://doi.org/10.1016/j.optmat.2021.111028.
40. I. Carlomagno, I. Lucarini, V. Secchi, F. Maita, D. Polese, S. Mirabella, G. Franzò, A. Notargiacomo, G. Di Santo, S. Gonzalez, L. Petaccia, L. Maiolo, *Appl. Surface Sci.* **587**, 152313 (2022) https://doi.org/10.1016/j.apsusc.2021.152313.

Вплив взаємодії інтенсивного УФ-випромінювання з тонкими плівками NZO

І.С. Вірт[1], Н.В. Барчук[1], П. Потера[2], М.В. Чекайло[3]

[1] *Дрогобицький державний педагогічний університет імені Івана Франка, 82100 Дрогобич, Україна*
[2] *Жешувський університет, 35-310 Жешув, Польща*
[3] *Національний університет "Львівська політехніка", 79000 Львів, Україна*

У даній роботі досліджено фізичні властивості тонких плівок оксиду цинку (зокрема, легованих нікелем NZO). Плівки вирощені як на жорстких, так і на гнучких підкладках за допомогою технології імпульсного лазерного напилення (PLD). У роботі показано та обговорено вплив параметрів та умов процесу фотонного відпалу на мікроструктурні, електричні та оптичні властивості наноструктури NZO. Після вирощення плівки відпалені УФ-випромінюванням. Результати показали, що процес відпалу суттєво змінив кристалічну структуру як в об'ємі, так і на поверхні. При оптимальній опроміненості 20 кДж/см^2 у випадку жорсткої підкладки та 36 кДж/см^2 у випадку гнучкої підкладки. Таким чином можна виготовити нову наноструктуровану поверхню з бажаними властивостями. Ці властивості контролюються в межах параметрів, що складаються з щільності потоку фотонів та часу експозиції. Дані дослідження підтверджують запропоновану модель поведінки дефектів для матеріалу ZnO та модель його електронних параметрів.

УФ-відпал є хорошою низькотемпературною технологією модифікації параметрів напівпровідника для застосування в гнучких пристроях. Зменшення дефектів по кисню узгоджується зі спостережуваною поведінкою вимірювальних електричних та оптичних характеристик. Одержані результати можуть стати важливою відправною точкою для розробки гнучких фотосенсорів та сумісної біоелектроніки.

Ключові слова: Оксид цинку, Тонкі плівки, Фотонний відпал, Морфологія поверхні, Електрофізичні вастивості, Фотоелектричні та Оптичні характеристики.